

ORIGINAL ARTICLE

Open Access



Ordered mesoporous carbon encapsulated linear poly(ionic liquid)s enabling synergy effect of surface groups and ionic moieties for CO₂ fixation under mild conditions

Yue Wu, Long Ma, Zhixin Song, Shu Dong, Zengjing Guo, Jun Wang* and Yu Zhou*

Abstract

Carbon dioxide (CO₂) fixation into value-added chemicals has attracted growing attention and one promising atom-efficient pathway is via the cycloaddition with three member-ring compounds like epoxides. Herein, we demonstrated that encapsulation of linear poly(ionic liquid)s (PILs) on ordered mesoporous carbon materials provides a facile and feasible approach towards environmental-friendly heterogeneous catalysts with high performance in CO₂ cycloaddition with epoxides under mild conditions. A series of novel linear phenolic hydroxyl group functional imidazolium-based PILs synthesized from hydroxymethylation reaction between 4-(imidazol-1-yl)phenol-1-butyl-imidazolium iodide and formaldehyde was loaded on ordered mesoporous carbon FDU-15–600 derived from mesoporous phenolic resin. By virtue of controlling the initial polymerization temperature, the molecular weight of PILs was facilely modulated, reaching strong host–guest interaction during the PIL immobilization. Highly stable immobilized PIL species with spatial satisfaction of ionic moieties and surface groups were thus realized to enable a synergic CO₂ conversion via cycloaddition with epoxides. The optimal catalyst exhibited high yield and stable recyclability by using atmospheric CO₂ under metal-additive-solvent-free conditions and the activity surprisingly exceeded the corresponding homogeneous parent IL and PIL. Excellent substrate compatibility was found by extending the transformation of more than ten epoxides including the inert ones such as disubstituted cyclohexene oxide. The significantly enhanced activity is attributed to the synergistic effect of the surface hydrogen groups and ionic moieties to accelerate the rate-determining ring-opening process.

Keywords: Carbon dioxide, cycloaddition reaction, Linear poly(ionic liquid)s, Ordered mesoporous carbon, Synergistic catalytic

1 Introduction

Carbon dioxide (CO₂) is one of the chief greenhouse gases causing growing global warming [1–4], and also an abundant inexpensive and nontoxic C1 feedstock [5, 6]. In this regard, chemically fixing CO₂ into high-value-added chemicals has attracted great attention in the mitigation of CO₂ emission [7–11]. One of the most promising

approaches is the cycloaddition reaction between CO₂ and three-member ring organic compounds such as aziridines and epoxides [12–14]. This pathway has the features of environmentally friendly and 100% atom-efficiency [5, 8, 15], producing a series of valuable chemicals like cyclic carbonates as solvents, polymer monomers, and organic intermediates [16–20]. To convert CO₂ molecules with inherent thermodynamic stability and kinetic inertness under mild condition [12, 21–23] encouraged the development of various homogeneous and heterogeneous catalysts including metal-porphyrin [6, 24], metal

*Correspondence: junwang@njtech.edu.cn; njutzhouyu@njtech.edu.cn

State Key Laboratory of Materials-Oriented Chemical Engineering, College of Chemical Engineering, Nanjing Tech University, Nanjing 210009, China

complexes [25, 26], metal–organic frameworks (MOFs) [27–29], covalent organic frameworks (COFs) [30, 31], ionic liquids (ILs) [32, 33], and porous organic polymers (POPs) [34–36], etc. The homogeneous catalysts normally exhibited high activity while the heterogeneous one allows facile catalyst separation and recycling. One of the dreaming ways to combine their advantages is the heterogenization of high-performance homogeneous catalysts but remains extremely challenging due to the potential activity decline and active sites leaching during this process.

Cycloaddition of CO₂ with epoxides usually undergoes ring opening, CO₂ insertion, and ring closure [37–39]. The first step is normally recognized as the rate-determining step and is triggered by an attack by a nucleophilic agent. The epoxide activation can be greatly promoted by Lewis acids (metal sites) [24–26, 28, 29] or hydrogen bond donors (HBDs) such as the hydroxyl group [5]. The anions of ILs were the efficient nucleophilic agents and the ILs' structure associating with the corresponding catalytic function can be facilely modulated at a molecular level by integrating versatile functional groups to promote CO₂ affinity and epoxide activation. Therefore, ILs and their derivatives have been extensively investigated as a large family of environmental-friendly metal-free catalysts for CO₂ cycloaddition [21, 40]. For example, phenolic hydroxyl group functional IL showed excellent activity in the CO₂ cycloaddition and achieved a high yield of 96% in the conversion of epichlorohydrin (ECH) at room temperature and atmospheric conditions [33]. To facilitate catalyst recycling, great efforts have been made to develop IL-related heterogeneous catalysts mainly comprising two following strategies [41–43]. One is the synthesis of ionic moieties containing polymers through the polymerization of IL monomer or with other linkers through various polymerization pathways such as free radical polymerization, hypercrosslinkage, and condensation [44–47]. For example, free radical self-polymerization of 2-(dimethylamino) ethyl methacrylate derived IL monomers afforded a series of PILs that can effectively catalyze the CO₂ cycloaddition with multiple epoxides with the yields of 70–98% at 110 °C and 20 bar [46]. Bifunctional ionic polymers were directly synthesized through co-polymerization of tris (4-vinylphenyl) phosphine and functional dibromides and the resulting carboxyl-containing one exhibited the yield above 99% at 140 °C in the transformation of atmospheric CO₂ via cycloaddition with ECH [47]. Alternatively, anchoring ILs and PILs on the porous materials provided a promising approach toward IL-derived solid materials that can inherit the abundant porosity of parent supports [8, 45]. More importantly, the combination of surface groups in the supports and immobilized

moieties favors reaching the highly effective synergistic conversion of CO₂ via cycloaddition with epoxide. Particularly, encapsulation of PILs on the ordered porous materials benefits to balance the stability and activity thanks to the confinement of the ordered porous channels and the spatial satisfaction of different reactive sites [48, 49]. This strategy is feasible and versatile for IL solidification because it does not rely on the designation of polymerizable IL monomer for the pore formation during the polymerization process. Many ordered porous materials with the large surface area such as zeolites, MOFs, COFs, and mesoporous silica have been explored to immobilize ILs and PILs for the preparation of heterogeneous IL-derived catalysts [16, 27, 28, 50]. Carbon materials with the features such as large surface area, tunable porosity, and abundant surface functional groups have been explored as the supports and catalysts in the CO₂ cycloadditions [51–57]. For instance, as a metal-free heterogeneous catalyst, graphene oxide (GOs) achieved 90.3% conversion and 98.6% selectivity in converting styrene oxide to styrene cyclic carbonate at 140 °C and 1 bar by using N,N-Dimethylformamide (DMF) as the solvent [55]. A PIL/graphene composite was prepared via an in-situ surface construction strategy and gave a yield of 99% in the coupling of 15 bar CO₂ with propylene oxide at 100 °C [56]. Carbon supported single Zn atom catalyst was constructed from the straightforward carbonization of carbon supported phenanthroline-ligated Zn(OAc)₂ complex and exhibited the yields of 93–98% in the conversion of seven epoxides via coupling with 5 bar CO₂ at 100 °C in the presence of tetrabutyl ammonium bromide (TBAB) as an additive [57]. The abundant surface oxygen groups such as hydroxyl groups on the carbon materials can serve as effective HBD to promote the epoxide activation to accelerate the corresponding transformation into the target cyclic carbonates [3, 41]. In addition to the disordered carbon materials mentioned above, ordered porous carbon materials such as CMK, FDU, and CGM-Cs (carbon-based Cornell Graded Materials) series [58–60]. Nonetheless, the encapsulation of PILs into the ordered porous carbon materials is still to be explored for the preparation of metal-free heterogeneous catalysts for CO₂-epoxide coupling.

Herein, we triggered the application of ordered mesoporous carbon materials in the encapsulation of linear PILs and constructed a family of facilely adjustable PIL-carbon hybrid heterogeneous catalysts for CO₂ fixation via cycloaddition with epoxide. The novel linear PILs were synthesized via hydroxymethylation reaction between phenolic hydroxyl functional imidazolium-based IL with formaldehyde solution under alkaline conditions [61], with molecular weight modulation via controlling the polymerization temperature. The target

ordered mesoporous carbon material FDU-15-600 was prepared through the carbonization of mesoporous phenolic resin that was synthesized in a soft-template route [62]. The linear PILs were confined in the mesochannels of FDU-15-600, reaching strong host-guest interaction that depended on the initial molecular weight of PILs. Herein, an effective synergy between the surface hydrogen groups and the ionic moieties with the nucleophilic agent was achieved and thus resulted in high efficiency in the cycloaddition of atmospheric CO₂ with epoxides under the mild condition without any additive and solvent. High yield, stable recycling performance and broad scope were observed in the catalysis evaluation. The activity of the champion heterogeneous PIL of the present work even outperformed its parent homogeneous IL and PIL, showing the great potential of this strategy.

1.1 Experimental section

1.1.1 Materials

The commercial chemicals and reagents were used as received without extra purification unless otherwise stated. 4-(Imidazol-1-yl) phenol (97%) was provided by Meyer (Shanghai) Chemical Technology Co. LTD. Iodobutane was provided by Xilong Science Co. LTD. Triblock copolymer (PEO-PPO-PEO, pluronic F127) was purchased from Sigma-Aldrich Co. LTD. Phenol was purchased from Shanghai Lingfeng Chemical Reagent Co. LTD. Activated carbon (AC) was purchased from Shanghai Macklin Biochemical Co. LTD.

1.1.2 Characterization

¹H nuclear magnetic resonance (NMR) spectra were collected on a Bruker DPX 500 spectrometer. C, H, and N combustion chemical analyses were performed on the Vario EL cube. Brunauer-Emmett-Teller (BET) surface areas and pore volumes were measured at the temperature of liquid nitrogen (-196 °C) by using a BELSORP-MINI analyzer. Prior to the measurement, all the samples were degassed at 150 °C for 3 h to a vacuum of 10⁻³ Torr. Scanning electron microscopy (SEM) images were acquired with a Hitachi S-4800 scanning electron microscope (10 kV). Transmission electron microscope (TEM) images were recorded on a JEOL JEM-2010 (200 kV) instrument. Small-angle X-ray diffraction (XRD) patterns were collected by using a Smart Lab X-ray diffractometer from Rigaku. Solid-state ¹³C cross-polarization (CP)/magic-angle-spinning (MAS) NMR (¹³C MAS NMR) analysis was carried out on a Bruker AVANCE-III spectrometer. X-ray photoelectron spectroscopy (XPS) spectra were collected on a PHI 5000 Versa Probe X-ray photoelectron spectrometer equipped with Al K α radiation (1486.6 eV). Thermal gravimetric analysis (TGA) experiments were performed on an STA409 instrument

under N₂ flow. The molecular weight of linear PILs was analyzed by gel permeation chromatography (GPC, 1515, Waters, USA). Raman spectra were collected on a Horiba HR 800 spectrometer with a Spectra-Physics 2018 Argon/Krypton Ion Laser system (excitation line: 514 nm).

1.1.3 Synthesis of soluble phenolic resol

Soluble phenolic resol was prepared under basic conditions according to a reported procedure [61]. Phenol (4.0 g, 42.5 mmol) was melted at 50 °C and then mixed with a sodium hydroxide solution (20 wt%, 0.85 g, 4.25 mmol) under stirring, followed by dropwise addition of formalin (37 wt%, 6.9 g, 85 mmol). The mixture was stirred at 75 °C for 1 h and then cooled to room temperature. The pH value of the solution above was adjusted to be 7.0 by using an aqueous hydrochloric acid solution with a concentration of 0.6 M. Subsequently, water was removed by rotary evaporation under vacuum and the resulting soluble phenolic resol was re-dissolved in ethanol for further use.

1.1.4 Synthesis of FDU-15-600

Triblock copolymer (PEO-PPO-PEO, pluronic F127; 0.6 g) was dissolved in ethanol (10.0 g) at 55 °C and then mixed with 3.0 g of ethanol solution containing soluble phenolic resol precursors (20 wt%). The mixture was stirred for 30 min to give a homogeneous solution, which was transferred to a 150 mm culture dish. Ethanol was evaporated at room temperature for 5–8 h. The resulting transparent membrane was then heated in an oven at 100 °C for 24 h. The obtained solids were calcined at 350 °C under nitrogen for 2 h with a heating rate of 1 °C min⁻¹ and then calcined at 600 °C for 3 h to afford FDU-15-600.

1.1.5 Synthesis of [p-ArOH-IM]I

The IL monomer [p-ArOH-IM]I was synthesized according to the reported procedure [33]. 4-(1-Imidazolyl) phenol (0.32 g, 2 mmol, 97%), *n*-Iodobutane (0.368 g, 2 mmol, 99%), and anhydrous alcohol (10 ml) were stirred at room temperature for 1 h and then heated at 100 °C for 24 h. The mixture was cooled to room temperature and washed with ethyl acetate (3 × 20 mL). The residue solvent was removed by rotary evaporation and the resulting solid was dried in a vacuum at 70 °C. ¹H NMR (400 MHz, Deuterium Oxide, Fig. S1): δ 9.08 (t, J = 1.7 Hz, 1H), 7.71 (t, J = 1.8 Hz, 1H), 7.60 – 7.51 (m, 1H), 7.47 – 7.35 (m, 2H), 7.05 – 6.93 (m, 2H), 4.23 (t, J = 7.2 Hz, 2H), 1.91 – 1.77 (m, 2H), 1.36 – 1.24 (m, 2H), 0.88 (t, J = 7.4 Hz, 3H).

1.1.6 Synthesis of linear PILs

In a typical synthesis, [*p*-ArOH-IM] I (0.162 g) and NaOH solution (20 wt%, 10 μ L) were mixed in a tube, followed by the addition of formaldehyde solution (37 wt%, 100 μ L). The mixture was sonicated for 30 min and then heated at 90 °C for 60 min. After that, the solution was neutralized by an aqueous HCl solution (0.6 M) and washed subsequently with ethanol and ethyl acetate to remove the residue [*p*-ArOH-IM]I and NaCl. The gel-like product was dried at 90 °C under vacuum to offer a linear PIL PIL-90. Varying the polymerization temperature to room temperature (RT), 55 °C, and 110 °C afforded PIL-RT, PIL-55, and PIL-110, respectively.

1.1.7 Preparation of FDU-15-600 supported linear PILs

Linear PIL was immobilized on FDU-15-600 by a wet-impregnation method. Typically, PIL-90 (0.089 g) was dissolved in ethanol (5 mL) to give a homogeneous solution, which was mixed with FDU-15-600 (0.504 g, pre-activated at 120 °C under vacuum for 3 h) in a 100 mL beaker. The mixture was stirred at room temperature for 12 h, with the auto-evaporation of ethanol, and then dried in a vacuum oven at 100 °C for 12 h to give the product 15%PIL-90@FDU-15-600. By varying the PIL precursor and the loading amount, various other hybrids were prepared.

1.1.8 Preparation of control samples

For comparison, several control samples, including 15%S-PIL-90@FDU-15-600, 15%PIL90@LOMC, 15%PIL-90@AC, and 15%IL@FDU-15-600 were prepared as follows.

15%S-PIL-90@FDU-15-600 Pre-activated FDU-15-600 (0.504 g), [*p*-ArOH-IM]I (0.086 g), and ethanol (5 mL) were mixed in a 50 mL flask and sonicated for 30 min to give the mixture A. An aqueous NaOH solution (20 wt%, 5 μ L) was diluted with formalin (37 wt%, 50 μ L) in a centrifuge tube and sonicated for 30 min to give the mixture B. The mixtures A and B were mixed in a 50 mL flask and stirred at 90 °C for 60 min under a nitrogen atmosphere. The resulting solid was dried in a vacuum oven at 100 °C for 12 h to give 15%S-PIL-90@FDU-15-600.

15%PIL-90@LOMC Disordered carbon (LOMC) was synthesized with the same procedure as that of FDU-15-600 except that more F127 (1 g) was involved. PIL-90 was loaded on LOMC with the same loading amount and procedure as that of 15%PIL-90@FDU-15-600 to give 15%PIL-90@LOMC.

15%PIL-90@AC 15%PIL-90@AC was prepared by loading PIL-90 with the same loading amount and procedure as that of 15%PIL-90@FDU-15-600.

15%IL@FDU-15-600 15%IL@FDU-15-600 was prepared by loading IL monomer [*p*-ArOH-IM]I on FDU-15-600 with the same loading amount and procedure to that of 15%PIL-90@FDU-15-600.

1.1.9 CO₂ cycloaddition with epoxide

The cycloaddition of atmospheric CO₂ with epoxides was carried out in a Schleck tube reactor (25 mL) equipped with a CO₂ balloon. Epoxide (5 mmol) and 15%PIL-90@FDU-15-600 (50 mg, 0.4 mol%) were stirred at the desired temperature for the preset time. After the reaction, the solid was separated by centrifugation and the internal standard *n*-dodecane (0.5 g) was added into the liquid phase, which was further diluted with ethyl acetate. The resulting solution was qualitatively analyzed by a gas chromatography-mass spectrometer (Bruker Scion 436 GC-MS) and quantitatively analyzed by a gas chromatograph (Agilent 7890B) equipped with a flame ionization detector (FID) and a capillary column (HP-5, 30 m \times 0.25 mm \times 0.25 μ m). The cycloaddition of high-pressure CO₂ with epoxide was conducted in a stainless-steel autoclave (25 mL) and the product was analyzed by GC and GC-MS as mentioned above.

The catalyst was isolated after the cycloaddition reaction, washed with ethyl acetate several times and dried at 90 °C for 12 h in a vacuum. Afterward, the catalyst was reused for the next catalytic run under the same reaction conditions. This procedure was repeated five times to examine the recyclability of the catalyst PIL-90@FDU-15-600.

2 Results and discussion

2.1 Structure of FDU-15-600 supported linear PIL

Scheme 1 depicts the preparation procedure of ordered mesoporous carbon confined linear PILs for CO₂ cycloaddition with epoxide. The ordered mesoporous carbon FDU-15-600 was synthesized by using F127 as the soft template and calcined at 350 °C to remove the template, with further carbonization at 600 °C. The linear PILs were synthesized via hydroxymethylation reaction, where [*p*-ArOH-IM]I bearing phenolic hydroxyl group and formaldehyde respectively served as the α -H resource component and a cross-linking agent [63, 64]. The linear PILs were immobilized on FDU-15-600 via the wet-impregnation process. By varying the polymerization temperature from room temperature (RT) to 110 °C, a series of linear PILs were synthesized and named PIL-*T*, where *T* = RT, 55, 90, and 110, represent

the polymerization temperature. As shown in Fig. S2, the color of the PIL-*T* series gradually become shallower with increasing polymerization temperature. CHN elemental analyses indicated that the PIL-*T* series had similar chemical composition to the IL precursor [*p*-ArOH-IM] I while slightly lower H content (Table S1 entries 1–5), attributable to the α -H elimination during the polymerization [40]. The polymerization degree of PIL-*T* was analyzed by gel permeation chromatography (GPC) (Fig. S3). The molecular weights of PIL-*T* were listed in Table 1. Polymerization at RT caused a low molecular weight that was about three times that of IL precursor (Table 1, entries 1 and 2), suggesting that PIL-RT was composed of about three [*p*-ArOH-IM]I molecules. With elevating polymerization temperature, the molecular weights of PIL-*T* series increased to 23,041, 30,494, and 48,084 at 55 °C, 90 °C, and 110 °C, respectively (Table 1, entries 3–5). This result implies that the polymerization degree of PIL-*T* was facily modulated by controlling the polymerization temperature.

A family of carbon encapsulated linear PIL samples, termed X%PIL-*T*@FDU-15–600 (X% index the loading amount), were prepared by using PIL-*T* with different

loading amounts, including 15%PIL-*T*@FDU-15–600, 10%PIL-90-FDU-15–600, and 20%PIL-90@FDU-15–600. There was no N element in FDU-15–600 and the detectable N species on X%PIL-*T*@FDU-15–600 samples reflected the immobilization of PIL-*T* (Table S1, entries 6–12). The PIL content linearly increased with the loading amount, while close to each other by fixing the loading amount. The small-angle XRD patterns of the parent FDU-15–600 and X%PIL-*T*@FDU-15–600 were displayed in Fig. 1a and Fig. S4a. For FDU-15–600, a strong diffraction peak was observed at the 2θ of 0.86, corresponding to the 100 plane [61]. Two weak peaks were found at the 2θ of 1.36 and 1.67, corresponding to the 110 and 200 planes [62]. The observation of these diffraction peaks revealed the formation of a well-ordered 2D hexagonal structure with a space group of *p6mm* [65]. The remaining of these peaks in the XRD patterns of X%PIL-*T*@FDU-15–600 indicated the preservation of the parent highly ordered hexagonal mesostructure after PIL-*T* loading. The weakening of the peak intensity came from the occupation of the guest PIL-*T* inside the meso-channels. The solid-state ^{13}C MAS NMR spectra of FDU-15–600 and the typical PIL loaded sample

Table 1 Textural properties

Entry	Sample	$S_{\text{BET}}^{\text{a}}$ ($\text{m}^2 \text{g}^{-1}$)	V_{p}^{b} ($\text{cm}^3 \text{g}^{-1}$)	D_{av}^{c} (nm)	IL content ^d (mmol g^{-1})	M_{n}^{e}
1	[<i>p</i> -ArOH-IM]I	-	-	-	2.89	344
2	PIL-RT	-	-	-	2.86	911
3	PIL-55	-	-	-	2.84	23,041
4	PIL-90	-	-	-	2.82	30,494
5	PIL-110	-	-	-	2.83	48,084
6	FDU-15–600	798	0.62	6.20	-	-
7	15%PIL-RT@FDU-15–600	336	0.30	6.20	0.37	-
8	15%PIL-55@FDU-15–600	301	0.30	6.20	0.39	-
9	15%PIL-90@FDU-15–600	283	0.29	6.20	0.40	-
10	15%PIL-110@FDU-15–600	261	0.29	6.20	0.39	-
11	10%PIL-90@FDU-15–600	547	0.37	6.20	0.28	-
12	20%PIL-90@FDU-15–600	238	0.26	6.20	0.50	-
13	AC	1526	0.52	1.40	-	-
14	15%PIL-90@AC	942	0.40	1.70	0.38	-
15	LOMC	674	0.45	4.20	-	-
16	15%PIL-90@LOMC	227	0.19	4.20	0.24	-
17	15%S-PIL-90@FDU-15–600	373	0.44	6.20	0.28	-
18	15%IL@FDU-15–600	252	0.28	5.52	0.37	-
19 ^f	15%PIL-90@FDU-15–600-R	282	0.30	6.20	0.38	-

^a BET surface area

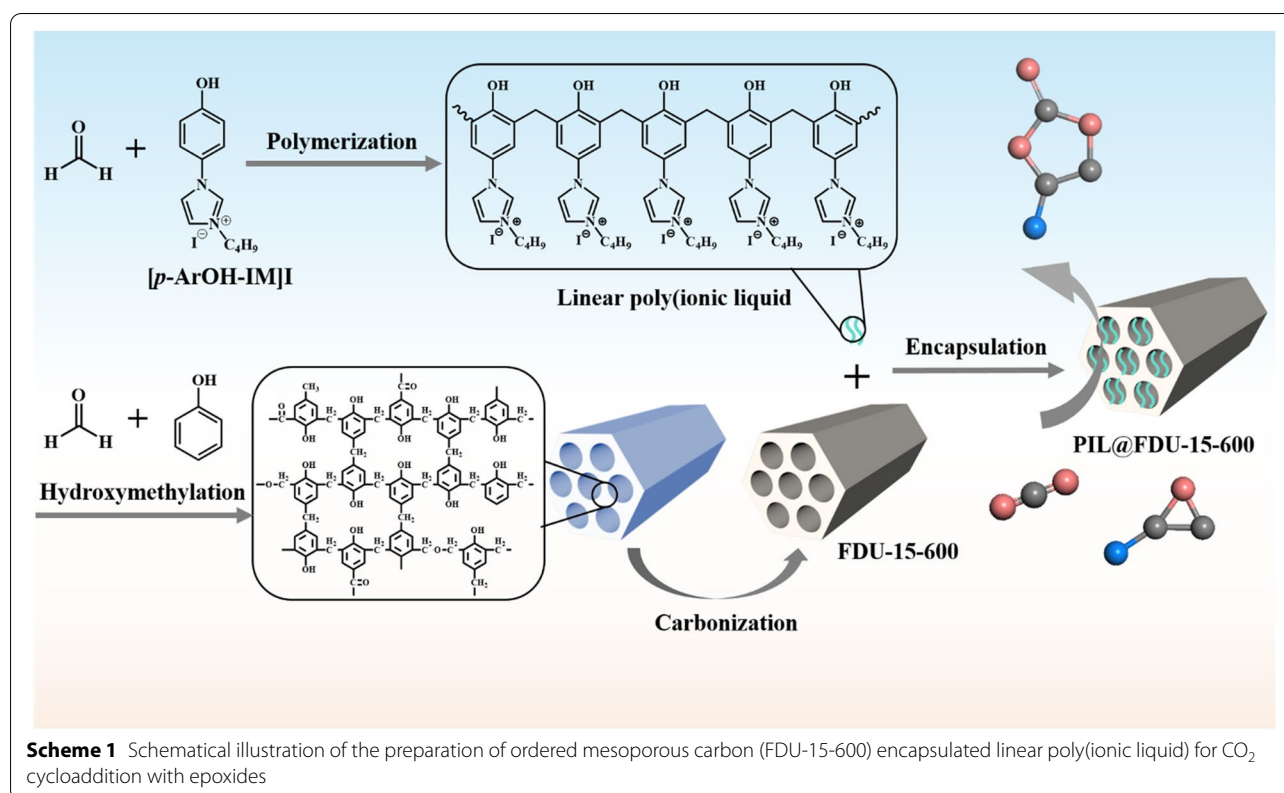
^b Total pore volume

^c Average pore size

^d Calculated from N content

^e Measured by gel permeation chromatography

^f Spent 15%PIL-90@FDU-15–600 recovered after the 5th run



15%PIL-90@FDU-15-600 were shown in Fig. 1b. Both of them exhibited similar and distinct peaks at ~ 28.1 , ~ 127 , and 153.4 ppm, which are respectively corresponded to the C atom of the methylene group linking the two benzene rings, the C atoms of the benzene ring adjacent the phenolic hydroxyl groups, and the other C atoms of the benzene ring [61, 63]. Comparing the spectrum of 15%PIL-90@FDU-15-600 with FDU-15-600, it was found that there existed an extra shoulder band at 138 ppm, attributable to the C2 atom of the imidazole ring [63]. This phenomenon is in line with the encapsulation of imidazolium based PIL in the FDU-15-600. Notably, a slight shift of the strong peak at 126.6 ppm to 127.4 ppm, which may be caused by the coincidence of the imaged C4 and C5 carbon atoms with the benzene ring carbon atoms, resulting in the change of the chemical shift of the characteristic peak of the aromatic carbon and imidazolium ring (C4 and C5 atoms) not obvious there [63].

Nitrogen sorption isotherms of FDU-15-600 and X%PIL-T@FDU-15-600 were investigated to provide the pore information (Fig. 1c). All of them displayed the typical IV type isotherm with an apparent H1-type hysteresis loop, characteristic of classical 2D-hexagonal mesopores [61, 64]. The pore size distribution curves calculated by using Barret-Joyner-Halenda (BJH) method

further visualized the existence of mesoporous structure (Fig. 1d). The Brunauer-Emmett-Teller (BET) surface areas and pore volumes were summarized in Table 1. FDU-15-600 had a high surface area of $798 \text{ m}^2 \text{ g}^{-1}$ and a large pore volume of $0.62 \text{ cm}^3 \text{ g}^{-1}$ (Table 1, entry 6). Decreased surface area and pore volume were observed after loading of PIL-T, and the higher loading, the less porosity (Table 1, entries 7–12). For example, the typical sample 15%PIL-90@FDU-15-600 has a surface area of $283 \text{ m}^2 \text{ g}^{-1}$ and a pore volume of $0.29 \text{ cm}^3 \text{ g}^{-1}$ (Table 1, entry 9). These results indicate that PIL-T occupies inside the mesopores.

X-ray photoelectron spectroscopy (XPS) analyses were performed to discern the interactions between the guests' PIL-X and the supports in 15%PIL-X@FDU-15-600 (X = RT, 55, 90, and 110). For comparison, FDU-15-600, [p-ArOH-IM]I, and 15%IL@FDU-15-600 were measured in parallel. The survey scan XPS spectrum of FDU-15-600 showed the signals at 284 and 532 eV for C1 and O1s species, respectively (Fig. S5a) [66]. Additional signals at 402 eV and 618 eV respectively for N1s and I3d species (Fig. S5a) were observed in the IL or PIL containing samples, reflecting the loading of these guests [67, 68]. The high-resolution N1s and I3d XPS (Figs. 2a and b) spectra indicated that [p-ArOH-IM]I exhibited one signal at 402.5 eV for N1s (N_1 species) and a set of double peaks at

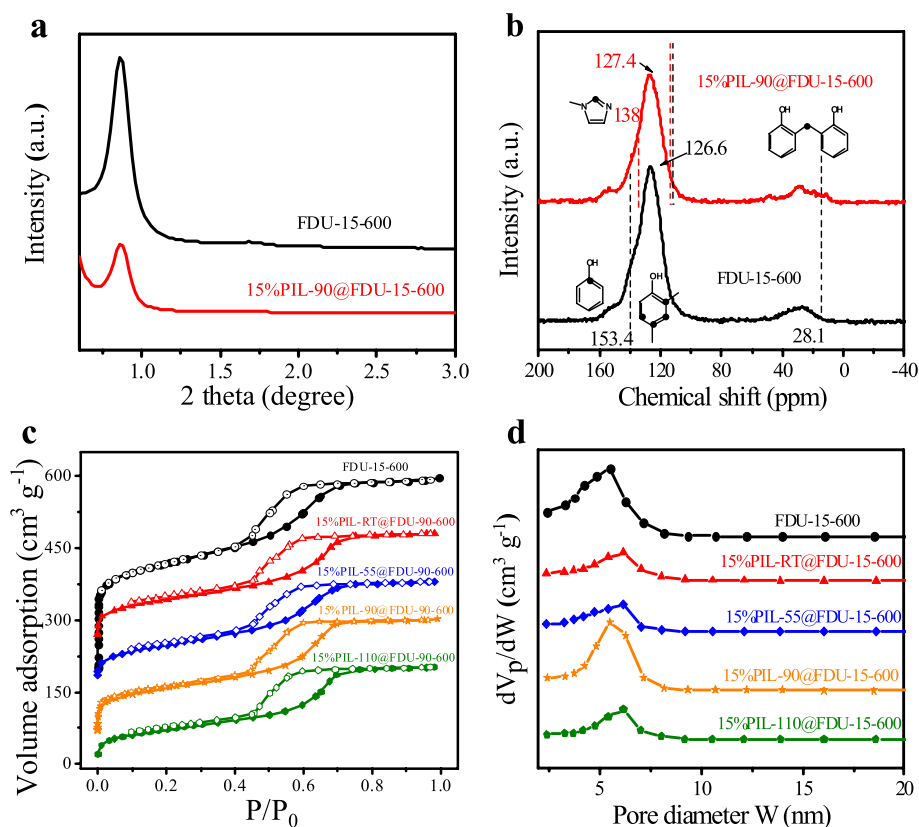


Fig. 1 **a** Small-angle XRD patterns. **b** Solid-state ^{13}C CP/MAS NMR spectra. **c** Nitrogen sorption isotherms and **d** pore size distribution curves. The sorption isotherms for samples FDU-15-600, 15%PILRT@FDU-15-600, 15%PIL-55@FDU-15-600, and 15%PIL-90@FDU-15-600 are shifted by 200, 250, 160, and $70\text{ cm}^3\text{ g}^{-1}$. The pore size distribution curves for samples FDU-15-600, 15%PIL-RT@FDU-15-600, 15%PIL-55@FDU-15-600, and 15%PIL-90@FDU-15-600 are shifted by 0.7, 0.55, 0.4, and $0.15\text{ cm}^3\text{ g}^{-1}$, respectively

630.8 eV for I3d(3/2) and 619.3 eV for I3d(5/2) (I_{I} species) [33, 69]. Loading [*p*-ArOH-IM]I on FDU-15-600 caused the emergence of one small N1s signal at 400.0 eV and a set of double I3d signals at 632.7/620.6 eV in the N1s and I3d XPS spectra of 15%IL@FDU-15-600, respectively. These signals came from the formation of less positively charged N species (N_{II}) and less negatively charged I species (I_{II}), attributable to the strong host-guest interaction that varied the cation-anion interaction in the immobilized [*p*-ArOH-IM]I on FDU-15-600. A similar phenomenon was observed in the N1s and I3d XPS spectra of 15%PIL-X@FDU-15-600. The proportion of different N and I species were calculated from their peak area and summarized in Table S2 and Table S3. More N_{II} and I_{II} species formed in 15%PIL-X@FDU-15-600 relative to 15%IL@FDU-15-600. With increasing polymerization temperature in the preparation of PIL precursor, the content of I_{II} species varied slightly, while the content of N_{II} species firstly increased and then decreased, reaching the maximum value at $T=90$ for 15%PIL-90@FDU-15-600. This result indicated that modulating the polymerization

temperature can facilitate the interaction between PIL and FDU-15-600, reaching a strong interaction at moderate polymerization temperature. The reason can be assigned that linear PIL with moderate molecular weight was synthesized under this condition, providing more binding sites to strengthen the host-guest interaction while avoiding the potential agglomeration by using the PIL precursor with excessive molecular weight. Besides, the O1s XPS spectra of all these samples were deconvoluted into two signals at 532 eV and 533 eV, respectively for C=O and C-OH species, proving the existence of hydroxyl species (Fig. S5b).

Additional characterizations were performed by taking the typical sample 15%PIL-90@FDU-15-600 as an example and the parent FDU-15-600 was tested in parallel to demonstrate the variation before and after immobilization of linear PIL. The morphology of FDU-15-600 and 15%PIL-90@FDU-15-600 were monitored by scanning electron microscopy (SEM) images (Fig. 3a and b). FDU-15-600 was composed of irregular particles on the micrometer scale, while 15%PIL-90@FDU-15-600

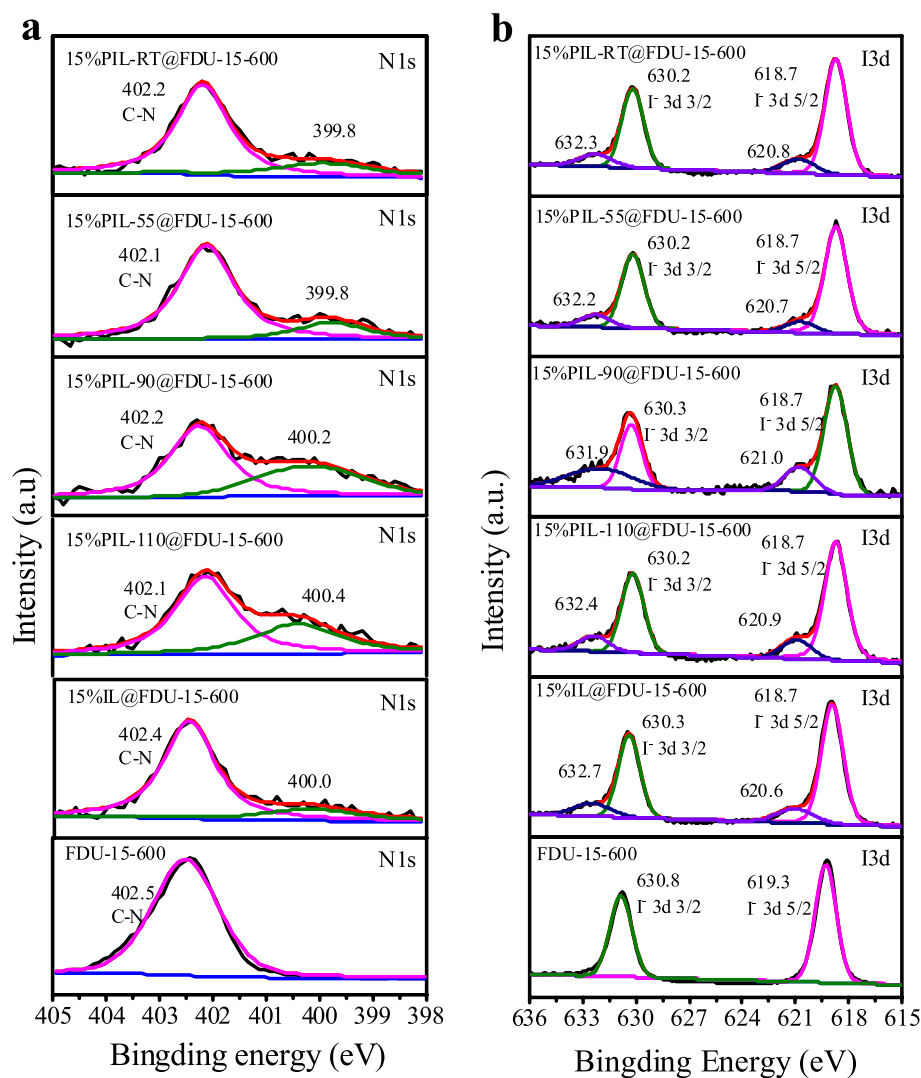


Fig. 2 a N1s and b I3d XPS spectra

demonstrated the almost same morphology. No spongy-like particles of the amorphous linear polymer were found, suggesting the formation of linear PIL inside FDU-15-600's mesopores. The transmission electron microscope (TEM) image of 15%PIL-90@FDU-15-600 shows the highly ordered mesoporous structure (Fig. 3c) [62, 63]. The corresponding elemental mapping images displayed the relatively homogeneous dispersion of C, N, O, and I elements, representative of the highly dispersive ionic moieties (Fig. 3d-g).

Thermogravimetric (TG) profiles of FDU-15-600, 15%PIL-90@FDU-15-600, and [*p*-ArOH-IM]I were presented in Fig. 4a and Fig. S6, showing negligible weight loss below 240 °C. Dramatical weight loss of 15%PIL-90@FDU-15-600 happened from 240 °C to 380 °C,

resembling the TG curve of [*p*-ArOH-IM]I (Fig. S6). This result suggests that the weight loss above came from the decomposition of the framework ionic moieties. What's more, the weight loss difference between FDU-15-600 and 15%PIL-90@FDU-15-600 was around 15%, close to the theoretical loading amount of PIL-90 and in line with the elemental analysis result (Table S1, entry 4). Raman spectra of FDU-15-600 and 15%PIL-90@FDU-15-600 were presented in Fig. 4b. Each Raman spectrum demonstrated two signals at 1336 cm^{-1} (D band) and 1587 cm^{-1} (G band) [61] respectively for the disordered carbon structure and graphitic domains [70]. The defect density is reflected by the ratio of the peak intensity of the D band to that of the G band (I_D/I_G). 15%PIL-90@FDU-15-600 exhibited slightly higher I_D/I_G values of 1.52 than

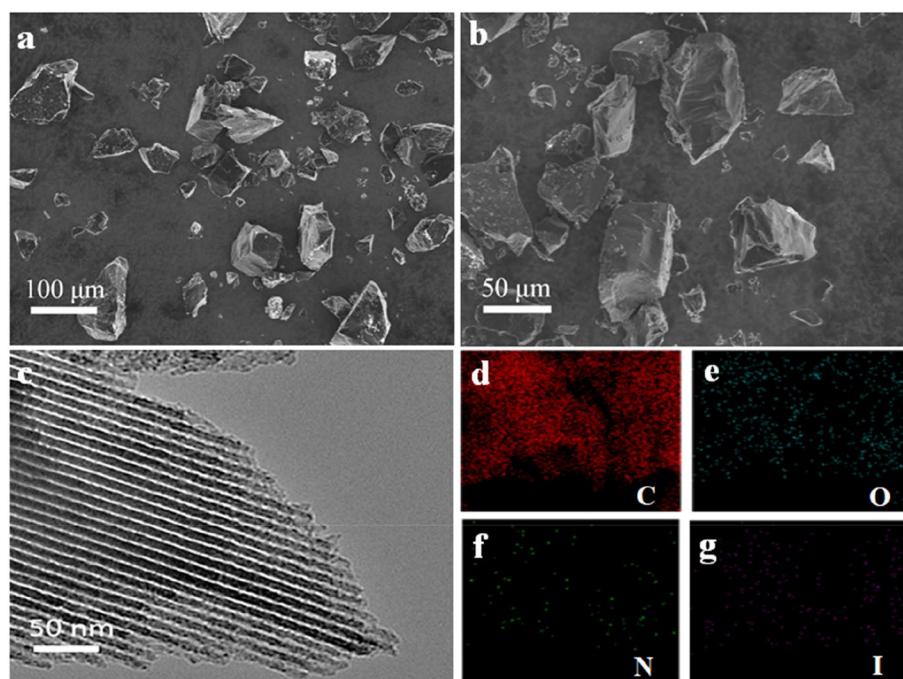


Fig. 3 SEM images of **a** FDU-15-600 and **b** 15%PIL-90@FDU-15-600. **c** TEM image of 15%PIL-90@FDU-15-600 and **d-g** corresponding elemental mapping images of C, O, N, and I, respectively

FDU-15-600 (1.46), which is assignable to the existence of an amorphous linear polymer in the meso-channels.

CO₂ adsorption isotherms of 15%PIL-X@FDU-15-600 were measured up to 1 bar at 298 K and compared with the ones of FDU-15-600 and 15%IL@FDU-15-600 (Fig. S7 and Fig. S8). These adsorption isotherms were fitted by using the Langmuir model [30] and the fitting parameters q_c and k_c of these samples were listed in Table S4, respectively corresponding to the saturated adsorption capacity of the adsorption site and the adsorption equilibrium constant. The CO₂ uptake at 1 bar was 2.16 mmol.g⁻¹ for FDU-15-600 and decreased after loading [*p*-ArOH-IM] I or PIL-*T* due to the decline of the surface area (Fig. 4c). The surface area normalized CO₂ uptakes at 1 bar was thus calculated to be 0.0027, 0.0030, 0.0021, 0.0028, 0.0040, and 0.0024 mmol.m⁻² for FDU-15-600, 15%IL@FDU-15-600, 15%PIL-X@FDU-15-600 (X = RT, 55, 90, and 110), respectively (Fig. 4d). 15%PIL-90@FDU-15-600 exhibited the highest surface area normalized CO₂ uptake, reflecting the favorable CO₂ trapping ability capacity.

2.2 CO₂ fixation through cycloaddition with epoxide

The catalytic performance of the above [*p*-ArOH-IM]I, PIL-*T*, and X%PIL-*T*@FDU-15-600 samples were evaluated in the CO₂ cycloaddition with epoxides to produce cyclic carbonates (Table 2). The investigation started

with CO₂ coupling with styrene oxide (SO) under a relatively mild condition of 110 °C and atmospheric pressure without any additive or solvent. For comparison, various control catalysts were tested in parallel, including the parent support FDU-15-600, IL precursor [*p*-ArOH-IM] I, and PIL-*T* series. FDU-15-600 was inactive in the reaction, giving a low yield of 2.6% (Table 2, entry 1). Feeding 0.4 mol% [*p*-ArOH-IM]I relative to SO led to a moderate yield of 80.0% and a turnover number (TON) of 200 (Table 2, entry 2). In parallel, the catalytic performance of PIL-*T* series and other solid catalysts below unless otherwise mentioned were tested by using the same dosage of ionic moieties to [*p*-ArOH-IM]I. The yield was 61.7% over PIL-RT and continuously increased along with the elevated polymerization temperature (Table 2, entry 3). Notably, the yield of PIL-90 (71.7%) was close to that of PIL-110 (72.6%), suggesting that excessive polymerization temperature caused only slight activity variation. Despite this, loading PIL-*T* on FDU-15-600 presented a different picture, with a maximum yield of 94.5% over 15%PIL-90@FDU-15-600. The influence of the reaction temperature and time was presented in Fig. S9, demonstrating a rapid increase in the yield with the temperature or time. Compared with previous encapsulated PILs catalysts (Table 3) [3, 27, 71], it is the first time to reach effective CO₂ cycloaddition with epoxides under atmospheric conditions over an encapsulated PIL catalyst.

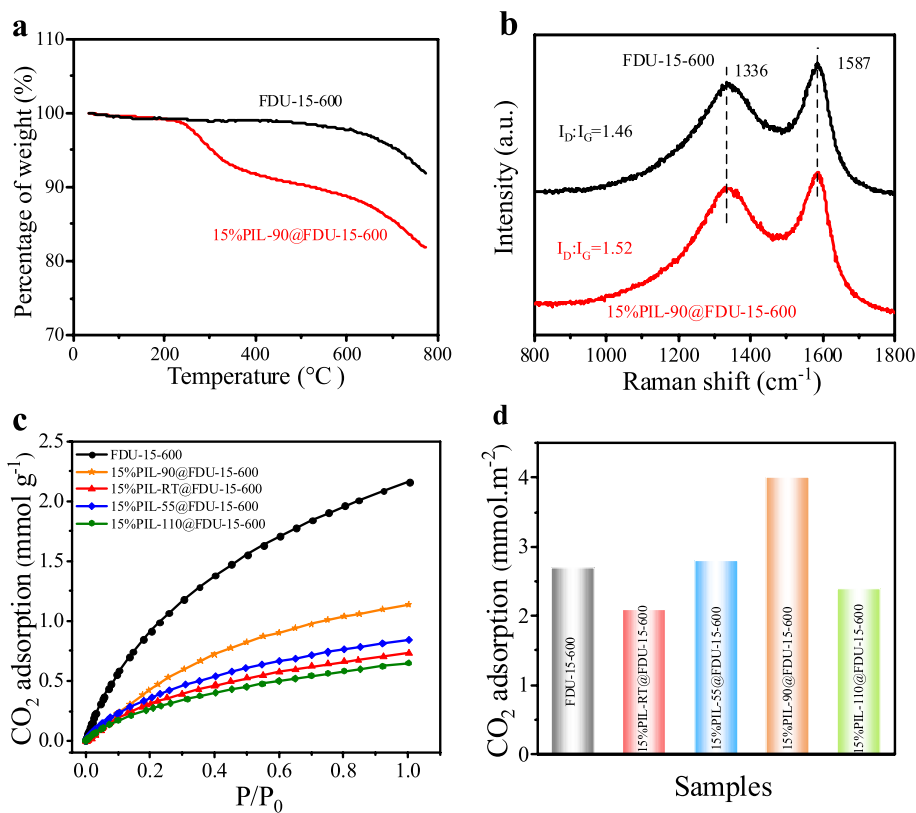


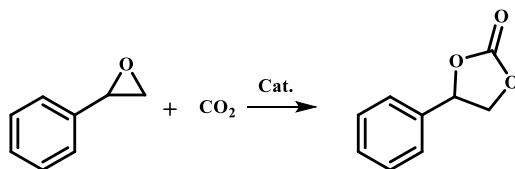
Fig. 4 **a** TG curves of FDU-15-600 and 15%PIL-90@FDU-15-600. **b** Raman spectra of FDU-15-600 and 15%PIL-90@FDU-15-600. **c** CO₂ adsorption isotherms at 298 K and **d** Unit adsorption capacity

Considering the substrate difference, Table 3 listed the activity involving various substrates. The comparison indicated that previous carbon supported IL or PIL catalysts can only catalyze the transformation of robust and moderate active substrates under high pressure [27, 42, 72–74]. By contrast, the scope surveying indicated the great substrate tolerance of 15%PIL-90@FDU-15-600, offering high yields even for those inert ones such as long-alkyl chain bearing terminal epoxide and disubstituted cyclohexene oxide under atmospheric condition, further demonstrating the superiority of this catalyst.

All the 15%PIL-T@FDU-15-600 catalysts showed a higher yield than the corresponding PIL-T sample and the activity of 15%PIL-90@FDU-15-600 is even superior to that of [*p*-ArOH-IM]I (Table 2, entries 2–10), revealing a synergistically catalytic process by combining the PIL-T and carbon support. Immobilization of PIL-110 on FDU-15-600 caused slight activity enhancement, assignable to the limited dispersion of the bulky linear polymer in a confined nano-space. In addition, the loading amount of PIL-90 on FDU-15-600 was explored by preparing two control samples with either lower (10%) or higher (20%) loading. The nitrogen sorption

result indicated a negative relationship between the loading amount and the porosity, i.e. the higher loading, the lower surface area and pore volume (Fig. S10 and Table 1, entries 9, 11, and 12). Varying the loading amount always provided a higher yield than the parent PIL-90 and moderate loading of 15% gave the highest activity when charging the same dosage of ionic moieties (Table 2, entries 9, 11, and 12), further reflecting the cooperation of PIL-90 and FDU-15-600. This is further supported by the result that 15%PIL-90@FDU-15-600 was more active than 15%PIL-90 + FDU-15-600, the physical mixture of FDU-15-600 and PIL-90 (yield: 94.5% vs 78.9%) (Table 2, entries 9 and 13).

For additional comparison, PIL-90 was impregnated on commercial activated carbon (AC) and a disordered carbon (LOMC) (Table S1, entries 13–16). AC is an amorphous carbon with a large surface area of 1526 m² g⁻¹ and a pore volume of 0.52 cm³ g⁻¹ (Fig. S11 and Table 1, entry 13). After loading with 15%PIL-90, the resulting sample 15%PIL-90@AC had a surface area of 942 m² g⁻¹ and a pore volume of 0.40 cm³ g⁻¹ (Table 1, entry 14). CO₂ cycloaddition with SO catalyzed by 15%PIL-90@AC gave a similar yield to PIL-90 (72.3% vs 71.7%) (Table 2, entry

Table 2 CO₂ cycloaddition with styrene oxide^a

Entry	Catalyst	Sel. ^b (%)	Yield ^b (%)	TON ^c
1	FDU-15-600	>99	2.6	-
2	[<i>p</i> -ArOH-IM]I	>99	80.0	200
3	PIL-RT	>99	61.7	154
4	PIL-55	>99	67.4	169
5	PIL-90	>99	71.7	179
6	PIL-110	>99	72.6	182
7	15%PIL-RT@FDU-15-600	>99	83.1	208
8	15%PIL-55@FDU-15-600	>99	87.2	218
9	15%PIL-90@FDU-15-600	>99	94.5	236
10	15%PIL-110@FDU-15-600	>99	80.5	201
11	10%PIL-90@FDU-15-600	>99	77.8	195
12	20%PIL-90@FDU-15-600	>99	76.6	192
13 ^d	15%PIL-90+FDU-15-600	>99	78.9	197
14	15%PIL-90@AC	>99	72.3	181
15	15%PIL-90@LOMC	>99	80.4	201
16	15%S-PIL-RT@FDU-15-600	>99	75.5	189
17	15%IL@FDU-15-600	>99	89.2	223
18 ^e	15%IL@FDU-15-600-R	>99	15.8	39.5
19 ^f	15%PIL-90@FDU-15-600-R	>99	89.9	225

^a Reaction conditions: styrene oxide (5 mmol), catalyst (0.4 mol%), 110 °C, 1 bar CO₂ (balloon), 24 h

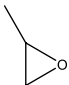
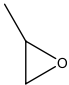
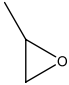
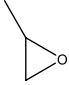
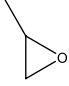
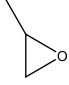
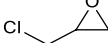

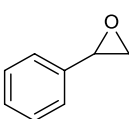


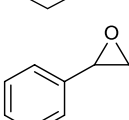
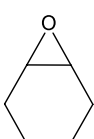
^b Selectivity and yield were determined by GC using dodecane as the internal standard

^c Turnover number (TON) = [mmol (product)]/[mmol (ionic sites)]

^d The same weight as 15%PIL-90@FDU-15-600. ^eSpent 15%IL@FDU-15-600 recovered after the 1st run

^f Spent 15%PIL-90@FDU-15-600 recovered after the 5th run

Table 3 Activity comparison with previous heterogeneous catalysts in CO₂ cycloaddition with epoxides

Entry	Catalyst	Epoxide	T (°C)	P (bar)	Yield (%)	TON	TOF (h ⁻¹)	Ref.
1	PIL-COF-100		90	10	99	252	10.5	[72]
2	PBIL-3		100	20	99	17.2	4.3	[75]
3	GO-H-Me		100	20	91.9	200	50	[71]
4	PPIL@COF-40		100	20	96	941	39	[76]
5	mSiO ₂ -PIL-3		120	20	99	23.1	3.8	[66]
6	5B-SiO ₂ -NH ₂ -3-I		110	20	99	313	52.2	[77]
7	Poly (HCO ₃ -OH-2)		80	1	95	111	4.63	[78]
8	Dm ₁ AOH ₄		130	15	91	568	227	[79]
9	SILEt ⁺ Br ⁻		110	20	44	583	117	[80]
10	15%PIL-90@FDU-15-600		110	1	99.7	249	10.4	This work
11	15%PIL-90@FDU-15-600		110	30	29.1	2645	7935	This work
12	15%PIL-90@FDU-15-600		110	1	94.5	236	9.8	This work
13	15%PIL-90@FDU-15-600		110	1	91.7	229	1.9	This work

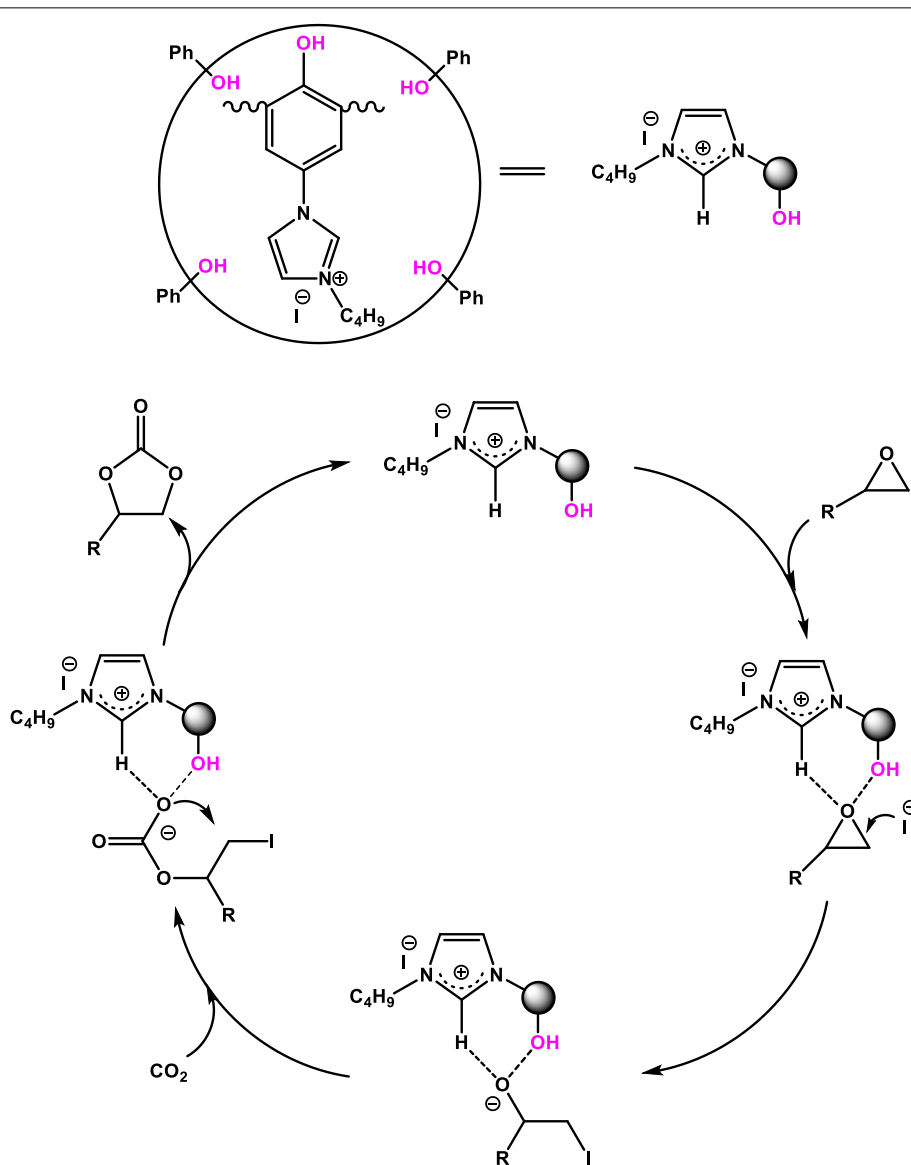
14), suggesting the lack of a synergistic effect between PIL-90 and AC. LOMC was derived from the carbonization of a disordered phenolic resin that was synthesized with the same procedure as that of FDU-15-600 except for the involvement of excessive soft-template F127. Small-angle XRD patterns of LOMC revealed a disordered structure, which was also observable on the sample 15%PIL-90@LOMC after loading with PIL-90 (Fig. S4b). Nitrogen sorption isotherm and pore size distribution

curve revealed the mesoporous structure of LOMC, with a similar surface area and pore volume to FDU-15-600 (Fig. S11 and Table 1, entry 15). Loaded sample 15%PIL-90@LOMC had a surface area of 227 m² g⁻¹ and a pore volume of 0.19 cm³ g⁻¹ (Table 1, entry 16). Under the identical reaction conditions, 15%PIL-90@LOMC exhibited a yield of 80.4% (Table 2, entry 15), close to that over [*p*-ArOH-IM]I but lower than the one over 15%PIL-90@FDU-15-600. These comparisons further reflect that

PIL-90 confined in an ordered meso-channels of FDU-15-600 resulted in the synergistic CO₂ cycloaddition with epoxide. The reason can be assigned to that the ordered meso-channels afforded the isolated nano-space to achieve better dispersion of these linear PILs, allowing the suitable distance between the surface groups of FDU-15-600 (for example, the hydroxyl groups) and ionic moieties. Besides, the in situ condensations of [*p*-ArOH-IM]I and formaldehyde on FDU-15-600 was conducted to provide a control sample 15%S-PIL-90@FDU-15-600, with a yield of 75.5% (Table 2, entry 16 and Table S1, entry 17). At the same time, it has 15% PIL-90@FDU-15-600. The similar specific surface area proves that the difference in activity comes from the different loading modes

(Table 1, entry 17). This phenomenon indicates that the immobilization of pre-polymerized PIL led to better dispersion for higher activity. Directly loading IL precursor [*p*-ArOH-IM]I on FDU-15-600 was conducted and the resulting sample 15%IL@FDU-15-600 (Figs. S12, S13, and Table S1, entry 18) offered a lower yield of 89.2% (Table 2, entry 17) than that of 15%PIL-90@FDU-15-600 and their specific surface areas are similar (Table 1, entry 18), further revealing the superiority of immobilization of PIL on this carbon support.

During the CO₂ cycloaddition with epoxide, the ring-opening is usually the rate-determining step and the epoxide activation can be promoted by the HBD through H-bond interaction [8, 21, 81–83]. For the supported ILs



Scheme 2 Proposed reaction route for CO₂ cycloaddition with epoxide catalyzed by 15%PIL-90@FDU-15-600

or PILs, the HBD species can come from the functional groups in ionic moieties and the support, but requiring spatial satisfactory [3, 14, 73, 84]. Previously, we have carefully investigated the role of phenolic hydroxyl group of imidazolium-based ILs in the cycloaddition with epoxide and afforded a highly active IL [*p*-ArOH-IM]I [33]. Herein, the heterogenization of this homogeneous IL was reached by first polymerization and successive loading on ordered mesoporous carbon FDU-15-600. The delocalized I⁻ anions of ionic moieties have well leaving ability, allowing superior spatial facilitation to complete the ring-opening with the assistance of HBD groups in the ionic moieties and surface groups. Based on the result above and previous mechanism investigation [19, 64, 85], the most probable reaction pathway is proposed for 15%PIL-90@FDU-15-600 catalyzed CO₂ cycloaddition with epoxide (Scheme 2), in which the I⁻ anions served as the nucleophilic reagent [40], while the abundant phenolic hydroxyl groups in the ionic moieties and inside the wall of mesochannels of FDU-15-600 acted as efficient HBD [5, 63, 86]. In the beginning, epoxide was adsorbed into the mesochannels of 15%PIL-90@FDU-15-600 and activated by the hydroxyl groups with the polarization of C–O bonds of epoxide through hydrogen bonding interaction [33, 40].

The nucleophilic attack of I⁻ anions to the C atom of activated epoxide led to the ring-opening, generating iodine-alkoxide followed by CO₂ insertion. After that, ring closure produced cyclic carbonate, with the left of I⁻ anions to regenerate the catalyst. The ring-opening is normally recognized as the rate-determining step [21], and the synergy of nucleophilic reagent and HBD is crucial for the epoxide activation and transition state stabilization [8, 33]. Modulating the molecular weight of PIL precursors can finely adjust the host–guest interaction to reach stable immobilization and favorable dispersion. Owing to this balance, the optimal sample 15%PIL-90@FDU-15-600 allowed the I⁻ anions to near the surface hydroxyl groups, satisfying the requirable synergistic effect. By contrast, the loading of IL precursor resulted in unstable active sites, showing apparent deactivation during the recycling test (Table 2, entry 18) due to the leaching of loaded IL molecules as demonstrated by the decline of the N content in the elemental analysis of the spent catalyst (Table S1, entry 19).

2.3 Reusability and scope

The recycling stability of a heterogeneous catalyst is of great importance for practical application. Delightedly, the separation of 15%PIL-90@FDU-15-600 from the

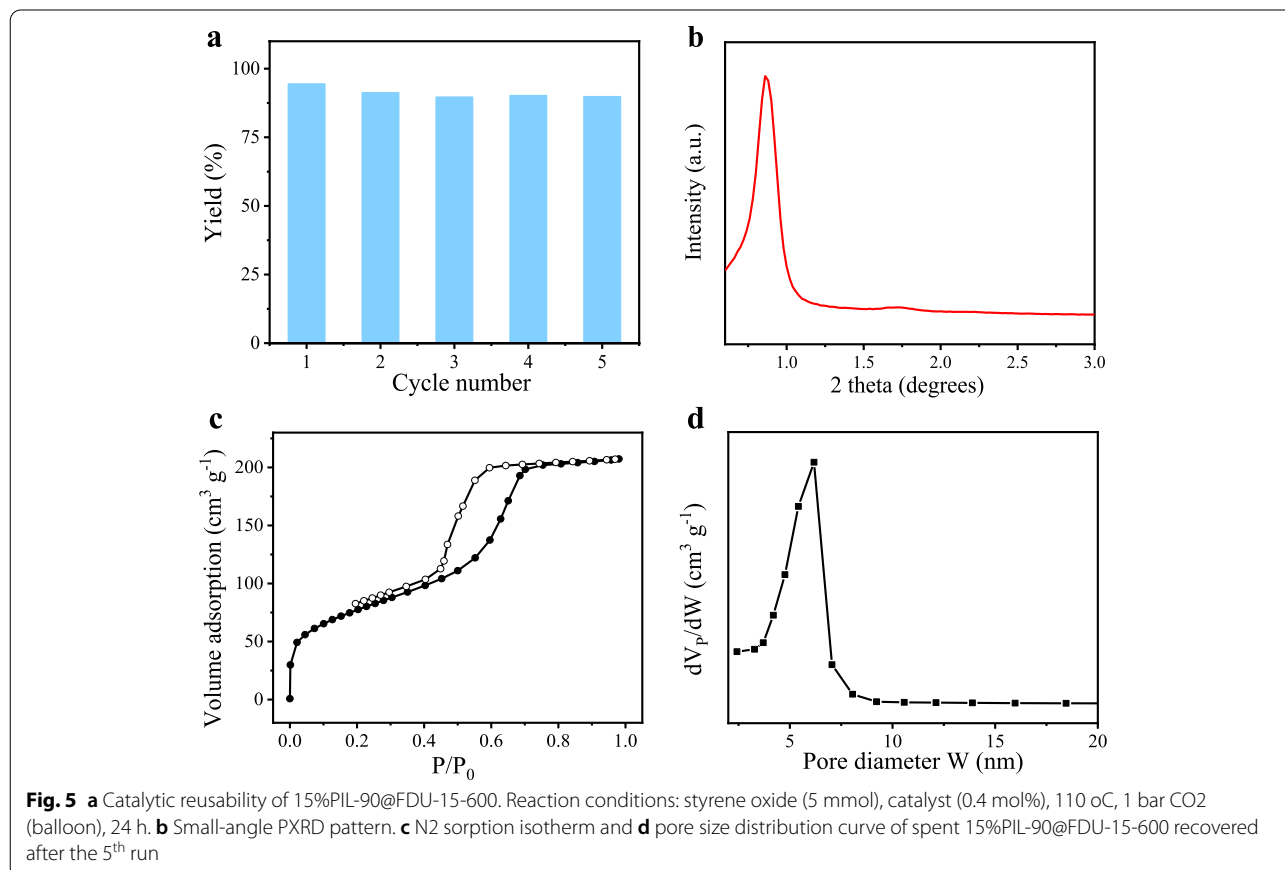


Table 4 CO₂ cycloaddition with epoxides catalyzed by 15%PIL-90@FDU-15-600^a

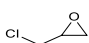
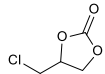
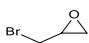
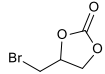
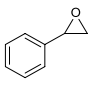
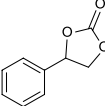
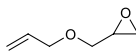
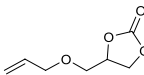
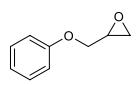
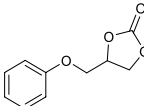
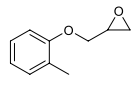
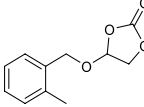
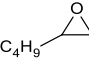
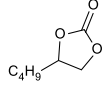
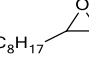
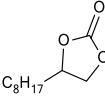
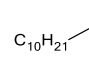
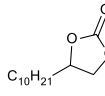
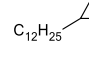
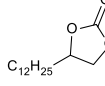
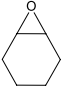
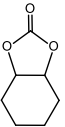

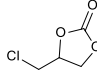
Entry	Substrate	Product	T (°C)	Sel. ^b (%)	Yield ^b (%)	TON ^c	TOF ^d (h ⁻¹)
1			110	>99	99.7	249	10.4
2			110	>99	96.7	242	10.1
3			110	>99	94.5	236	9.8
4			110	>99	84.5	211	8.8
5			110	>99	89.0	222	9.3
6			110	>99	92.7	232	9.7
7 ^e			110	>99	98.2	123	2.6
8 ^e			110	>99	96.7	121	2.5
9 ^e			110	>99	90.5	113	2.4
10 ^e			110	>99	96	120	2.5
11 ^f			110	>99	91.7	115	0.9
12 ^g			120	>99	29.1	2645	7935

Table 4 (continued)^a Reaction condition: epoxides (5 mmol), catalyst (0.4 mol%), 1 bar CO₂ (balloon), 24 h^b Conversion and selectivity were determined by GC using dodecane as the internal standard^c Turnover number (TON) = [mmol (product)]/[mmol (ionic sites)]^d Turnover frequency (TOF) = [mmol (product)]/[mmol (ionic sites) × (reaction time)]^e Reaction condition: epoxides (5 mmol), catalyst (0.8 mol%), 1 bar CO₂ (balloon), 48 h^f Reaction condition: epoxides (5 mmol), catalyst (0.8 mol%), 1 bar CO₂ (balloon), 120 h^g Reaction condition: epoxide (21 mmol), catalyst (0.011 mol%), 3 MPa CO₂, 20 min

reaction mixture was readily realized by facile centrifugation. Recycling investigation showed that the catalytic activity of 15%PIL-90@FDU-15-600 was well retained during the 5 runs test in CO₂ cycloaddition with SO (Fig. 5a and Table 2, entry 19). The ordered mesopores and structural integrity was observed by recording the small angle XRD and specific surface area (Table 1, entry 19) pattern of the spent 15%PIL-90@FDU-15-600 recovered after the 5th run (Fig. 5b). The preservation of the chemical composition and porosity during the recycling cycloaddition with epoxide was evidenced by the almost same elemental analysis result (Table S1, entry 20), N₂ sorption isotherm and the pore size distribution curve (Figs. 5c and 5d) of the spent 15%PIL-90@FDU-15-600 as the fresh one. All of these are responsive to excellent recyclability and stability.

The scope 15%PIL-90@FDU-15-600 was extended to the CO₂ fixation with various epoxides (Table 4). Good to excellent yields were achieved in these terminal epoxides comprising the ones containing long alkyl chains, the conversion of which was more difficult than those active epoxides like epichlorohydrin (Table 4, entries 1–10) [3, 41]. Notably, the effective cycloaddition of atmospheric CO₂ with inert disubstituted cyclohexene oxide over the present catalyst afforded a high yield of 91.7% (Table 4, entry 11). This is rarely reached by heterogeneous catalysts before [3, 40]. The scope surveying indicated the great substrate tolerance of this catalyst. It is worth mentioning that a high TON of 2645 and turnover frequency (TOF) of 7935 (Table 4, entry 12) was observed over 15%PIL-90@FDU-15-600 by using high pressure CO₂ (3 MPa), greatly outperforming those carbon encapsulated ILs and PILs listed in Table 3. Though various effective heterogeneous catalysts with high TON and TOF have been reported before, it is still scarcely for metal-free heterogeneous catalysts under additive and solve free conditions. A comprehensive comparison with previous catalysts under similar conditions [3, 45, 81–83] indicated that the above TON and TOF over 15%PIL-90@FDU-15-600 under harsh conditions are superior to majority of those state-of-art ones, and particularly, a record-high TOF was reached over this metal-free catalyst. All of these reveal the high performance of 15%PIL-90@FDU-15-600 in the heterogeneous CO₂ cycloaddition with epoxides.

3 Conclusion

A family of linear PILs with tunable molecular weight was synthesized through a hydroxy methylation reaction between a phenolic hydroxyl group functional imidazolium-based IL and formaldehyde by controlling the polymerization temperature. The resulting PILs were encapsulated on the mesoporous phenolic resin derived ordered mesoporous carbon FDU-15-600 to give the corresponding heterogeneous PIL-carbon hybrid catalysts. The interaction between PILs and carbon was strengthened by involving PIL with moderate molecular weight synthesized using moderate polymerization temperature. Not only the stability was improved, but also the suitable spatial adjacency of the ionic moieties and surface groups in the wall of mesochannels was reached, affording synergistically catalytic CO₂ cycloaddition with epoxide. The best-performing catalyst was highly active in the transformation of a series of epoxides through coupling with CO₂ under the atmospheric condition without any metal species, additive or solvent, and even more active than the parent IL and PIL precursors. The catalyst was readily recovered and reused, and stable activity was observable during the recycling test. This work provides a facile and feasible perspective toward IL-derived heterogeneous catalysts and highlights the great potential of ordered mesoporous carbon materials in the rational designation of highly effective metal-free catalysts for CO₂ fixation.

Abbreviations

AC: Activated carbon; LOMC: Disordered carbon; Triblock copolymer: PEO-PPO-PEO, pluronic F127.

Supplementary Information

The online version contains supplementary material available at <https://doi.org/10.1007/s43979-022-00041-5>.

Additional file 1: Fig. S1. ¹H NMR spectrum of [p-ArOH-IM]. **Fig. S2.** Optical images of PIL-RT, PIL-55, PIL-90, and PIL-110. **Fig. S3.** GPC spectra of PIL-RT, PIL-55, PIL-90, and PIL-110. **Fig. S4.** Small-angle XRD patterns of (a) FDU-15-600 encapsulated PILs and (b) various control samples. **Fig. S5.** (a) Survey scan and (b) O1s XPS spectra. **Fig. S6.** TG curve of [p-ArOH-IM] I under N₂ atmosphere. **Fig. S7.** CO₂ adsorption isotherms of 15%IL@FDU-15-600 at 298 K. **Fig. S8.** CO₂ adsorption isotherms at 298 K of (a) FDU-15-600, (b) 15%IL@FDU-15-600, (c) 15%PIL-RT@FDU-15-600, (d) 15%PIL-55@FDU-15-600, (e) 15%PIL-90@FDU-15-600, and (f) 15%PIL-110@FDU-15-600. **Fig. S9.** Yield as a function of (a) reaction temperature and (b)

reaction time in 15%PIL-90@FDU-15-600 catalyzed CO₂ cycloaddition with styrene oxide. Reaction conditions: styrene oxide (5 mmol), 15%PIL-90@FDU-15-600 (0.4 mol %), 1 bar CO₂ (balloon). **Fig. S10.** (a) N₂ sorption isotherms and (b) pore size distribution curves of 10%PIL-90@FDU-15-600 and 20%PIL-90@FDU-15-600. **Fig. S11.** (a) Nitrogen sorption isotherms and (b) pore size distribution curves. The sorption isotherms for samples AC, 15%PIL-90@AC, LOMC, and 15%PIL-90@LOMC are shifted by 220, 230, 200, and 210 cm³ g⁻¹. The pore size distribution curves for samples AC, 15%PIL-90@AC, LOMC, and 15%PIL-90@LOMC are shifted by 1.2, 0.9, 0.5, and 0.3 cm³ g⁻¹, respectively. **Fig. S12.** Small-angle XRD pattern of 15%L@FDU-15-600. **Fig. S13.** (a) N₂ sorption isotherm and (b) pore size distribution curve of 15%L@FDU-15-600. **Table S1.** Elemental analysis^a. **Table S2.** Types and content of N in the samples. **Table S3.** Types and content of I in the samples. **Table S4.** Fitting parameters for the CO₂ sorption isotherms^a.

Acknowledgements

The computational resources generously provided by the High-Performance Computing Center of Nanjing Tech University are greatly appreciated.

Authors' contributions

YW conducted the investigation and wrote the original draft. LM contributed on the experiment design, test and written of original draft. ZS, SD and ZG conducted partial experiments and data analysis. JW and YZ conceived and supervised the project and revised the manuscript. All authors read and approved the final manuscript.

Funding

Open access funding provided by Shanghai Jiao Tong University. This work was supported by the National Natural Science Foundation of China (grants 22072065, 22178162, and 22222806), the Distinguished Youth Foundation of Jiangsu Province (BK20220053), and the Six Talent Peaks Project in Jiangsu Province (grant JNH-B-035).

Availability of data and materials

Not applicable.

Declarations

Ethics approval and consent to participate

Not applicable.

Consent for publication

Not applicable.

Competing interests

The authors declare that they have no known competing financial interests or personal relationships that could have appeared to influence the work reported in this paper.

Received: 21 October 2022 Revised: 7 November 2022 Accepted: 15 November 2022

Published online: 03 January 2023

References

- Zhu X, Xie W, Wu J, Miao Y, Xiang C, Chen C, Ge B, Gan Z, Yang F, Zhang M, O'hare D, Li J, Ge T, Wang R (2022) Recent advances in direct air capture by adsorption. *Chem Soc Rev* 51(15):6574–6651. <https://doi.org/10.1039/d1cs00970b>
- Singh G, Lee J, Karakoti A, Bahadur R, Yi J, Zhao D, Albahily K, Vinu A (2020) Emerging trends in porous materials for CO₂ capture and conversion. *Chem Soc Rev* 49(13):4360–4404. <https://doi.org/10.1039/d0cs00075b>
- Li G, Dong S, Fu P, Yue Q, Zhou Y, Wang J (2022) Synthesis of porous poly(ionic liquid)s for chemical CO₂ fixation with epoxides. *Green Chem* 24(9):3433–3460. <https://doi.org/10.1039/d2gc00324d>
- Wang S, Wang Y, Kuang Y, Xu S, Gao S, Liu L, Niu H, Xiao P, Huang B (2022) Adsorption behaviour of molecular sieve and activated carbon for CO₂ adsorption at cold temperatures. *Carbon Neutrality* 1(1):16. <https://doi.org/10.1007/s43979-022-00017-5>
- Guo Z, Jiang Q, Shi Y, Li J, Yang X, Hou W, Zhou Y, Wang J (2017) Tethering Dual Hydroxyls into Mesoporous Poly(ionic liquid)s for Chemical Fixation of CO₂ at Ambient Conditions: A Combined Experimental and Theoretical Study. *ACS Catal* 7(10):6770–6780. <https://doi.org/10.1021/acscatal.7b02399>
- Deacy AC, Kilpatrick AFR, Regoutz A, Williams CK (2020) Understanding metal synergy in heterodinuclear catalysts for the copolymerization of CO₂ and epoxides. *Nat Chem* 12(4):372–380. <https://doi.org/10.1038/s41557-020-0450-3>
- Zhou Y, Zhang J, Wang L, Cui X, Liu X, Wong SS, An H, Yan N, Xie J, Yu C, Zhang P, Du Y, Xi S, Zheng L, Cao X, Wu Y, Wang Y, Wang C, Wen H, Chen L, Xing H, Wang J (2021) Self-assembled iron-containing mordenite monolith for carbon dioxide sieving. *Science* 373:315–320. <https://doi.org/10.1126/science.aax5776>
- Jia D, Ma L, Wang Y, Zhang W, Li J, Zhou Y, Wang J (2020) Efficient CO₂ enrichment and fixation by engineering micropores of multifunctional hypercrosslinked ionic polymers. *Chem Eng J* 390:124652. <https://doi.org/10.1016/j.cej.2020.124652>
- Zhai G, Liu Y, Mao Y, Zhang H, Lin L, Li Y, Wang Z, Cheng H, Wang P, Zheng Z, Dai Y, Huang B (2022) Improved photocatalytic CO₂ and epoxides cycloaddition via the synergistic effect of Lewis acidity and charge separation over Zn modified UiO-bpydc. *Appl Catal B* 301:120793. <https://doi.org/10.1016/j.apcatb.2021.120793>
- Cheng J, Cen K (2022) Mechanisms of strengthening energy and mass transfer in microbial conversion of flue-gas-derived CO₂ to biodiesel and biogas fuels. *Carbon Neutrality* 1(1):11. <https://doi.org/10.1007/s43979-022-00004-w>
- Chernyak SA, Corda M, Dath JP, Ordosky VV, Khodakov AY (2022) Light olefin synthesis from a diversity of renewable and fossil feedstocks: state-of-the-art and outlook. *Chem Soc Rev* 51(18):7994–8044. <https://doi.org/10.1039/d1cs01036k>
- Xu G-Q, Ma X-N, Jia X-B, Dong Y-H, Jiang Y-Q, Li X-J (2022) Synthesis of nucleoside-substituted carbonate and diol derivatives through the carbon dioxide reaction using polyionic liquid catalysts. *Green Chem* 24(11):4573–4580. <https://doi.org/10.1039/d2gc00566b>
- Chen SJ, Li JS, Haddad R, Sadeghzadeh SM (2022) Cycloaddition of allylic chlorides, aryl alkynes, and carbon dioxide using nanoclusters of polyoxomolybdate buckyball supported by ionic liquid on dendritic fibrous nanosilica. *J CO₂ Util* 61:10235. <https://doi.org/10.1016/j.jcou.2022.102035>
- Zhou Y, Zhang W, Ma L, Zhou Y, Wang J (2019) Amino Acid Anion Paired Mesoporous Poly(ionic liquids) as Metal-/Halogen-Free Heterogeneous Catalysts for Carbon Dioxide Fixation. *ACS Sustainable Chem Eng* 7(10):9387–9398. <https://doi.org/10.1021/acssuschemeng.9b00591>
- Li J, Jia D, Guo Z, Liu Y, Lyu Y, Zhou Y, Wang J (2017) Imidazolium based porous hypercrosslinked ionic polymers for efficient CO₂ capture and fixation with epoxides. *Green Chem* 19(11):2675–2686. <https://doi.org/10.1039/c7gc00105c>
- Dan M, Zhong R, Hu S, Wu H, Zhou Y, Liu Z-Q (2022) Strategies and challenges on selective electrochemical hydrogen peroxide production: Catalyst and reaction medium design. *Chem Catal* 2(8):1919–1960. <https://doi.org/10.1016/j.checat.2022.06.002>
- Tong H, Qu Y, Li Z, He J, Zou X, Zhou Y, Duan T, Liu B, Sun J, Guo K (2022) Halide-free pyridinium saccharinate binary organocatalyst for the cycloaddition of CO₂ into epoxides. *Chem Eng J* 444:135478. <https://doi.org/10.1016/j.cej.2022.135478>
- Luo R, Yang Y, Chen K, Liu X, Chen M, Xu W, Liu B, Ji H, Fang Y (2021) Tailored covalent organic frameworks for simultaneously capturing and converting CO₂ into cyclic carbonates. *J Mater Chem A* 9(37):20941–20956. <https://doi.org/10.1039/d1ta05428g>
- Guo L, Lamb KJ, North M (2021) Recent developments in organocatalysed transformations of epoxides and carbon dioxide into cyclic carbonates. *Green Chem* 23(1):77–118. <https://doi.org/10.1039/d0gc03465g>
- Guo YC, Chen WJ, Feng L, Fan YC, Liang JS, Wang XM, Zhang X (2022) Greenery-inspired nanoengineering of bamboo-like hierarchical porous nanotubes with spatially organized bifunctionalities for synergistic photothermal catalytic CO₂ fixation. *J Mater Chem A* 10(23):12418–12428. <https://doi.org/10.1039/d2ta02885a>

21. Yang GW, Xu CK, Xie R, Zhang YY, Zhu XF, Wu GP (2021) Pinwheel-Shaped Tetranuclear Organoboron Catalysts for Perfectly Alternating Copolymerization of CO₂ and Epichlorohydrin. *J Am Chem Soc* 143(9):3455–3465. <https://doi.org/10.1021/jacs.0c12425>
22. Gong L, Sun J, Liu Y, Yang G (2021) Photoinduced synergistic catalysis on Zn single-atom-loaded hierarchical porous carbon for highly efficient CO₂ cycloaddition conversion. *J Mater Chem A* 9(38):21689–21694. <https://doi.org/10.1039/d1ta06159c>
23. Meng X, Ju Z, Zhang S, Liang X, Von Solms N, Zhang X, Zhang X (2019) Efficient transformation of CO₂ to cyclic carbonates using bifunctional protic ionic liquids under mild conditions. *Green Chem* 21(12):3456–3463. <https://doi.org/10.1039/c9gc01165j>
24. Luo R, Chen M, Zhou F, Zhan J, Deng Q, Yu Y, Zhang Y, Xu W, Fang Y (2021) Synthesis of metalloporphyrin-based porous organic polymers and their functionalization for conversion of CO₂ into cyclic carbonates: recent advances, opportunities and challenges. *J Mater Chem A* 9(46):25731–25749. <https://doi.org/10.1039/d1ta08146b>
25. Yang Q, Yang CC, Lin CH, Jiang HL (2019) Metal-Organic-Framework-Derived Hollow N-Doped Porous Carbon with Ultrahigh Concentrations of Single Zn Atoms for Efficient Carbon Dioxide Conversion. *Angew Chem Int Ed* 58(11):3511–3515. <https://doi.org/10.1002/anie.201813494>
26. Sinha I, Lee Y, Bae C, Tussupbayev S, Lee Y, Seo M-S, Kim J, Baik M-H, Lee Y, Kim H (2017) Computer-aided rational design of Fe(III)-catalysts for the selective formation of cyclic carbonates from CO₂ and internal epoxides. *Catal Sci Technol* 7(19):4375–4387. <https://doi.org/10.1039/c7cy01435j>
27. Ding M, Jiang H-L (2018) Incorporation of Imidazolium-Based Poly(ionic liquid)s into a Metal-Organic Framework for CO₂ Capture and Conversion. *ACS Catal* 8(4):3194–3201. <https://doi.org/10.1021/acscatal.7b03404>
28. Sun Y, Huang H, Vardhan H, Aguila B, Zhong C, Perman JA, Al-Enizi AM, Nafady A, Ma S (2018) Facile Approach to Graft Ionic Liquid into MOF for Improving the Efficiency of CO₂ Chemical Fixation. *ACS Appl Mater Interfaces* 10(32):27124–27130. <https://doi.org/10.1021/acsmi.8b08914>
29. Yuan Y, Li J, Sun X, Li G, Liu Y, Verma G, Ma S (2019) Indium-Organic Frameworks Based on Dual Secondary Building Units Featuring Halogen-Decorated Channels for Highly Effective CO₂ Fixation. *Chem Mater* 31(3):1084–1091. <https://doi.org/10.1021/acs.chemmater.8b04792>
30. Cao JJ, Shan WJ, Wang Q, Ling XC, Li G, Lyu Y, Zhou Y, Wang J (2019) Ordered Porous Poly(ionic liquid) Crystallines: Spacing Confined Ionic Surface Enhancing Selective CO₂ Capture and Fixation. *ACS Appl Mater Interfaces* 11(6):6031–6041. <https://doi.org/10.1021/acsmi.8b19420>
31. Zhi Y, Shao P, Feng X, Xia H, Zhang Y, Shi Z, Mu Y, Liu X (2018) Covalent organic frameworks: efficient, metal-free, heterogeneous organocatalysts for chemical fixation of CO₂ under mild conditions. *J Mater Chem A* 6(2):374–382. <https://doi.org/10.1039/c7ta08629f>
32. Liu J, Yang G, Liu Y, Zhang D, Hu X, Zhang Z (2020) Efficient conversion of CO₂ into cyclic carbonates at room temperature catalyzed by Al-salen and imidazolium hydrogen carbonate ionic liquids. *Green Chem* 22(14):4509–4515. <https://doi.org/10.1039/d0gc00458h>
33. Guo Z, Hu Y, Dong S, Chen L, Ma L, Zhou Y, Wang L, Wang J (2022) "Spring-loaded" mechanism for chemical fixation of carbon dioxide with epoxides. *Chem Catal* 2(3):519–530. <https://doi.org/10.1016/j.cheecat.2021.12.023>
34. Kong L, Han S, Zhang T, He L, Zhou L (2021) Developing hierarchical porous organic polymers with tunable nitrogen base sites via theoretical calculation-directed monomers selection for efficient capture and catalytic utilization of CO₂. *Chem Eng J* 420:127621. <https://doi.org/10.1016/j.cej.2020.127621>
35. Wang X, Dong Q, Xu Z, Wu Y, Gao D, Xu Y, Ye C, Wen Y, Liu A, Long Z, Chen G (2021) Hierarchically nanoporous copolymer with built-in carbene-CO₂ adducts as halogen-free heterogeneous organocatalyst towards cycloaddition of carbon dioxide into carbonates. *Chem Eng J* 403:126460. <https://doi.org/10.1016/j.cej.2020.126460>
36. Cui C, Sa R, Hong Z, Zhong H, Wang R (2020) Ionic-Liquid-Modified Click-Based Porous Organic Polymers for Controlling Capture and Catalytic Conversion of CO₂. *ChemSuschem* 13(1):180–187. <https://doi.org/10.1002/cssc.201902715>
37. Qu Y, Chen Y, Sun J (2022) Conversion of CO₂ with epoxides to cyclic carbonates catalyzed by amino acid ionic liquids at room temperature. *J CO₂ Util* 56:101840. <https://doi.org/10.1016/j.jcou.2021.101840>
38. Park S, Morales-Collazo O, Freeman B, Brennecke JF (2022) Ionic Liquid Stabilizes Olefin Facilitated Transport Membranes Against Reduction. *Angew Chem Int Ed* 61(25):e202202895. <https://doi.org/10.1002/anie.202202895>
39. Xin X, Shan H, Tian T, Wang Y, Yuan D, You H, Yao Y (2020) Conversion of CO₂ into Cyclic Carbonates under Ambient Conditions Catalyzed by Rare-Earth Metal Complexes Bearing Poly(phenolato) Ligand. *ACS Sustainable Chem Eng* 8(35):13185–13194. <https://doi.org/10.1021/acssuschemeng.0c01736>
40. Bobbink FD, Vasilyev D, Hulla M, Chamam S, Menoud F, Laurenczy G, Katsyuba S, Dyson PJ (2018) Intricacies of Cation-Anion Combinations in Imidazolium Salt-Catalyzed Cycloaddition of CO₂ Into Epoxides. *ACS Catal* 8(3):2589–2594. <https://doi.org/10.1021/acscatal.7b04389>
41. Wang X, Zhou Y, Guo Z, Chen G, Li J, Shi Y, Liu Y, Wang J (2015) Heterogeneous conversion of CO₂ into cyclic carbonates at ambient pressure catalyzed by ionothermal-derived meso-macroporous hierarchical poly(ionic liquid)s. *Chem Sci* 6(12):6916–6924. <https://doi.org/10.1039/c5sc02050f>
42. Kojčinović A, Likozar B, Grilc M (2022) Heterogeneous catalytic materials for carboxylation reactions with CO₂ as reactant. *J CO₂ Util* 66:102250. <https://doi.org/10.1016/j.jcou.2022.102250>
43. Song H, Wang Y, Liu Y, Chen L, Feng B, Jin X, Zhou Y, Huang T, Xiao M, Huang F, Gai H (2021) Conferring Poly(ionic liquid)s with High Surface Areas for Enhanced Catalytic Activity. *ACS Sustainable Chem Eng* 9(5):2115–2128. <https://doi.org/10.1021/acssuschemeng.0c07399>
44. Singh SK, Savoy AW (2020) Ionic liquids synthesis and applications: An overview. *J Mol Liq* 297:112038. <https://doi.org/10.1016/j.jmolliq.2019.112038>
45. Liu M, Wang X, Jiang Y, Sun J, Arai M (2018) Hydrogen bond activation strategy for cyclic carbonates synthesis from epoxides and CO₂: current state-of-the-art of catalyst development and reaction analysis. *Catal Rev* 61(2):214–269. <https://doi.org/10.1080/01614940.2018.1550243>
46. Ying T, Tan X, Su Q, Cheng W, Dong L, Zhang S (2019) Polymeric ionic liquids tailored by different chain groups for the efficient conversion of CO₂ into cyclic carbonates. *Green Chem* 21(9):2352–2361. <https://doi.org/10.1039/c9gc00010k>
47. Wan YL, Zhang ZM, Ding C, Wen LL (2021) Facile construction of bifunctional porous ionic polymers for efficient and metal-free catalytic conversion of CO₂ into cyclic carbonates. *J CO₂ Util* 52:101673. <https://doi.org/10.1016/j.jcou.2021.101673>
48. Du YR, Xu BH, Xia SP, Ding GR, Zhang SJ (2021) Dehydrative Formation of Isosorbide from Sorbitol over Poly(ionic liquid)-Covalent Organic Framework Hybrids. *ACS Appl Mater Interfaces* 13(1):552–562. <https://doi.org/10.1021/acsmi.0c18105>
49. Sun Q, Aguila B, Perman J, Nguyen N, Ma S (2016) Flexibility Matters: Cooperative Active Sites in Covalent Organic Framework and Threaded Ionic Polymer. *J Am Chem Soc* 138(48):15790–15796. <https://doi.org/10.1021/jacs.6b10629>
50. Aguila B, Sun Q, Wang X, O'roure E, Al-Enizi AM, Nafady A, Ma S (2018) Lower Activation Energy for Catalytic Reactions through Host-Guest Cooperation within Metal-Organic Frameworks. *Angew Chem Int Ed* 57(32):10107–10111. <https://doi.org/10.1002/anie.201803081>
51. Buaki-Sogó M, Vivian A, Bivona LA, García H, Gruttadauria M, Aprile C (2016) Imidazolium functionalized carbon nanotubes for the synthesis of cyclic carbonates: reducing the gap between homogeneous and heterogeneous catalysis. *Catal Sci Technol* 6(24):8418–8427. <https://doi.org/10.1039/c6cy01068g>
52. Polidoro D, Perosa A, Rodríguez-Castellón E, Canton P, Castoldi L, Rodríguez-Padrón D, Selva M (2022) Metal-Free N-Doped Carbons for Solvent-Less CO₂ Fixation Reactions: A Shrimp Shell Valorization Opportunity. *ACS Sustainable Chem Eng* 10(41):13835–13848. <https://doi.org/10.1021/acssuschemeng.2c04443>
53. Gbe J-LK, Ravi K, Singh M, Neogi S, Grafonté M, Biradar AV (2022) Hierarchical porous nitrogen-doped carbon supported MgO as an excellent composite for CO₂ capture at atmospheric pressure and conversion to value-added products. *J CO₂ Util* 65:102222. <https://doi.org/10.1016/j.jcou.2022.102222>
54. Zhong H, Yang C, Fan L, Fu Z, Yang X, Wang X, Wang R (2019) Dyadic promotion of photocatalytic aerobic oxidation via the Mott-Schottky effect enabled by nitrogen-doped carbon from imidazolium-based ionic polymers. *Energy Environ Sci* 12(1):418–426. <https://doi.org/10.1039/c8ee02727g>
55. Zhang S, Zhang H, Cao F, Ma Y, Qu Y (2018) Catalytic Behavior of Graphene Oxides for Converting CO₂ into Cyclic Carbonates at One

- Atmospheric Pressure. *ACS Sustainable Chem Eng* 6(3):4204–4211. <https://doi.org/10.1021/acssuschemeng.7b04600>
56. Guo XX, Zhang FL, Muhammad Y, Hu DL, Cai ZT, Xiao GM (2022) Enhancement in the active site exposure in a porphyrin-based PIL/graphene composite catalyst for the highly efficient conversion of CO₂. *Dalton Trans* 51(8):3331–3340. <https://doi.org/10.1039/d1dt04338b>
 57. Cui X, Dai X, Surkus A-E, Junge K, Kreyenschulte C, Agostini G, Rockstroh N, Beller M (2019) Zinc single atoms on N-doped carbon: An efficient and stable catalyst for CO₂ fixation and conversion. *Chin J Catal* 40(11):1679–1685. [https://doi.org/10.1016/s1872-2067\(19\)63316-4](https://doi.org/10.1016/s1872-2067(19)63316-4)
 58. Hesse SA, Beaucage PA, Smilgies DM, Wiesner U (2021) Structurally Asymmetric Porous Carbon Materials with Ordered Top Surface Layers from Nonequilibrium Block Copolymer Self-Assembly. *Macromolecules* 54(6):2979–2991. <https://doi.org/10.1021/acs.macromol.0c02720>
 59. Jeong U, Kim H, Ramesh S, Dogan NA, Wongwilawan S, Kang S, Park J, Cho ES, Yavuz CT (2021) Rapid Access to Ordered Mesoporous Carbons for Chemical Hydrogen Storage. *Angew Chem Int Ed* 60(41):22478–22486. <https://doi.org/10.1002/anie.202109215>
 60. Jeong Y, Cui M, Choi J, Lee Y, Kim J, Son Y, Khim J (2020) Development of modified mesoporous carbon (CMK-3) for improved adsorption of bisphenol-A. *Chemosphere* 238:124559. <https://doi.org/10.1016/j.chemosphere.2019.124559>
 61. Meng Y, Gu D, Zhang F, Shi Y, Yang H, Li Z, Yu C, Tu B, Zhao D (2005) Ordered Mesoporous Polymers and Homologous Carbon Frameworks: Amphiphilic Surfactant Templating and Direct Transformation. *Angew Chem Int Ed* 117(43):7215–7221. <https://doi.org/10.1002/ange.200501561>
 62. Liu F, Huang K, Wu Q, Dai S (2017) Solvent-Free Self-Assembly to the Synthesis of Nitrogen-Doped Ordered Mesoporous Polymers for Highly Selective Capture and Conversion of CO₂. *Adv Mater* 29(27):2932–2941. <https://doi.org/10.1002/adma.201700445>
 63. Zhang W, Wang Q, Wu H, Wu P, He M (2014) A highly ordered mesoporous polymer supported imidazolium-based ionic liquid: an efficient catalyst for cycloaddition of CO₂ with epoxides to produce cyclic carbonates. *Green Chem* 16(11):4767–4774. <https://doi.org/10.1039/c4gc01245c>
 64. Zhang W, Mei Y, Wu P, Wu H-H, He M-Y (2019) Highly tunable periodic imidazole-based mesoporous polymers as cooperative catalysts for efficient carbon dioxide fixation. *Catal Sci Technol* 9(4):1030–1038. <https://doi.org/10.1039/c8cy02595a>
 65. Nie D, Liang Y, Zhou T, Sun Q, Shi G, Jin L (2012) FDU-15-Pt composites with different Pt loading and their electrocatalytic reduction to ultratrace nitroaromatic compounds. *Int J Environ Anal Chem* 92(7):832–843. <https://doi.org/10.1080/03067319.2010.520124>
 66. Yang C, Chen Y, Wang X, Sun J (2022) Polymeric ionic liquid with carboxyl anchored on mesoporous silica for efficient fixation of carbon dioxide. *J Colloid Interface Sci* 618:44–55. <https://doi.org/10.1016/j.jcis.2022.03.066>
 67. Demirci S, Yurddaskal M, Dikici T, Sarioglu C (2018) Fabrication and characterization of novel iodine doped hollow and mesoporous hematite (Fe₂O₃) particles derived from sol-gel method and their photocatalytic performances. *J Hazard Mater* 345:27–37. <https://doi.org/10.1016/j.jhazmat.2017.11.009>
 68. Muniandy L, Adam F, Rahman NRA, Ng E-P (2019) Highly selective synthesis of cyclic carbonates via solvent free cycloaddition of CO₂ and epoxides using ionic liquid grafted on rice husk derived MCM-41. *Inorg Chem Commun* 104:1–7. <https://doi.org/10.1016/j.inoche.2019.03.012>
 69. Li K, Zhao Y, Zhang P, He C, Deng J, Ding S, Shi W (2016) Combined DFT and XPS investigation of iodine anions adsorption on the sulfur terminated (001) chalcopyrite surface. *Appl Surf Sci* 390:412–421. <https://doi.org/10.1016/j.apsusc.2016.08.095>
 70. Shan W, Li S, Cai X, Zhu J, Zhou Y, Wang J (2018) Carbon catalyzed hydroxylation of benzene with dioxygen to phenol over surface carbonyl groups. *ChemCatChem* 11:1076–1085. <https://doi.org/10.1002/cctc.201801668>
 71. Lan D-H, Gong Y-X, Tan N-Y, Wu S-S, Shen J, Yao K-C, Yi B, Au C-T, Yin S-F (2018) Multi-functionalization of GO with multi-cationic ILs as high efficient metal-free catalyst for CO₂ cycloaddition under mild conditions. *Carbon* 127:245–254. <https://doi.org/10.1016/j.carbon.2017.11.007>
 72. Du Y-R, Yang X, Wang Y-F, Guan P-X, Wang R, Xu B-H (2022) Immobilization poly(ionic liquid)s into hierarchical porous covalent organic frameworks as heterogeneous catalyst for cycloaddition of CO₂ with epoxides. *Mol Catal* 520:112164. <https://doi.org/10.1016/j.mcat.2022.112164>
 73. Lan DH, Fan N, Wang Y, Gao X, Zhang P, Chen L, Au CT, Yin SF (2016) Recent advances in metal-free catalysts for the synthesis of cyclic carbonates from CO₂ and epoxides. *Chin J Catal* 37(6):826–845. [https://doi.org/10.1016/S1872-2067\(15\)61085-3](https://doi.org/10.1016/S1872-2067(15)61085-3)
 74. Lian S, Song C, Liu Q, Duan E, Ren H, Kitamura Y (2021) Recent advances in ionic liquids-based hybrid processes for CO₂ capture and utilization. *J Environ Sci* 99:281–295. <https://doi.org/10.1016/j.jes.2020.06.034>
 75. Yang CK, Chen YL, Qu Y, Zhang JX, Sun JM (2021) Phase-controllable polymerized ionic liquids for CO₂ fixation into cyclic carbonates. *Sustain Energ Fuels* 5(4):1026–1033. <https://doi.org/10.1039/d0se01293a>
 76. Du Y-R, Ding G-R, Wang Y-F, Xu B-H, Zhang S-J (2021) Construction of a PPI@COF core-shell composite with enhanced catalytic activity for CO₂ conversion. *Green Chem* 23(6):2411–2419. <https://doi.org/10.1039/d1gc00267h>
 77. Ye Y, Chen Y, Huang J, Sun J (2022) In-situ Synthesis of Ionic Liquids on B-doped Mesoporous SiO₂ Catalyst for Epoxide-CO₂ Cycloaddition. *Asian J Org Chem* 11(8):e202200234. <https://doi.org/10.1002/ajoc.202200234>
 78. Jiang B, Liu J, Yang G, Zhang Z (2022) Efficient conversion of CO₂ into cyclic carbonates under atmospheric by halogen and metal-free Poly(ionic liquid)s. *Chin J Chem Eng*. <https://doi.org/10.1016/j.cjche.2022.05.018>
 79. Červenková Štátná L, Krupková A, Petrickovic R, Müllerová M, Matoušek J, Koštejn M, Cuřínová P, Jandová V, Šabata S, Strašák T (2020) Multivalent Bifunctional Carbosilane Dendrimer-Supported Ammonium and Phosphonium Organocatalysts for the Coupling of CO₂ and Epoxides. *ACS Sustainable Chem Eng* 8(31):11692–11703. <https://doi.org/10.1021/acssuschemeng.0c03367>
 80. Dokhaee Z, Ghiaci M, Farrokhpour H, Buntkowsky G, Breitzke H (2020) SBA-15-Supported Imidazolium Ionic Liquid through Different Linkers as a Sustainable Catalyst for the Synthesis of Cyclic Carbonates: A Kinetic Study and Theoretical DFT Calculations. *Ind Eng Chem Res* 59(28):12632–12644. <https://doi.org/10.1021/acs.iecr.0c01050>
 81. Shaikh RR, Pornpraprom S, Delia V (2017) Catalytic Strategies for the Cycloaddition of Pure, Diluted, and Waste CO₂ to Epoxides under Ambient Conditions. *ACS Catal* 8(1):419–450. <https://doi.org/10.1021/acscatal.7b03580>
 82. Xu B-H, Wang J-Q, Sun J, Huang Y, Zhang J-P, Zhang X-P, Zhang S-J (2015) Fixation of CO₂ into cyclic carbonates catalyzed by ionic liquids: a multi-scale approach. *Green Chem* 17(1):108–122. <https://doi.org/10.1039/c4gc01754d>
 83. Luo R, Liu X, Chen M, Liu B, Fang Y (2020) Recent Advances on Imidazolium-Functionalized Organic Cationic Polymers for CO₂ Adsorption and Simultaneous Conversion into Cyclic Carbonates. *Chemoschem* 13:3945–3966. <https://doi.org/10.1002/cssc.202001079>
 84. Zhou X, Weber J, Yuan J (2019) Poly(ionic liquid)s: Platform for CO₂ capture and catalysis. *Curr Opin Green Sustainable Chem* 16:39–46. <https://doi.org/10.1016/j.cogsc.2018.11.014>
 85. Wang JQ, Dong K, Cheng WG, Sun J, Zhang SJ (2012) Insights into quaternary ammonium salts-catalyzed fixation carbon dioxide with epoxides. *Catal Sci Technol* 2(7):1480–1484. <https://doi.org/10.1039/c2cy20103h>
 86. Toda Y, Komiyama Y, Kikuchi A, Suga H (2016) Tetraarylphosphonium Salt-Catalyzed Carbon Dioxide Fixation at Atmospheric Pressure for the Synthesis of Cyclic Carbonates. *ACS Catal* 6(10):6906–6910. <https://doi.org/10.1021/acscatal.6b02265>